Inverse Design of Few-Layer Metasurfaces Empowered by the Matrix Theory of Multilayer Optics

Zhancheng Li,[1] Wenwei Liu,[1] Dina Ma,[1] Shiwang Yu,[1] Hua Cheng,[1,*] Duk-Yong Choi,[2] Jianguo Tian,[1] and Shuqi Chen[1,3,4,†]

[1] *The Key Laboratory of Weak Light Nonlinear Photonics, Ministry of Education, Renewable Energy Conversion and Storage Center, School of Physics and TEDA Institute of Applied Physics, Nankai University, Tianjin 300071, China*

[2] *Laser Physics Centre, Research School of Physics and Engineering, Australian National University, Canberra ACT 2601, Australia*

[3] *The Collaborative Innovation Center of Extreme Optics, Shanxi University, Taiyuan, Shanxi 030006, China*

[4] *Collaborative Innovation Center of Light Manipulations and Applications, Shandong Normal University, Jinan 250358, China*

(Received 12 September 2021; revised 7 November 2021; accepted 11 January 2022; published 2 February 2022)

Few-layer metasurfaces, which are planar artificial arrays composed of more than one functional layer, have been showing unprecedented capabilities for the implementation of integrated and miniaturized optical devices with high efficiency and broad working bandwidth. However, the rich design freedoms of few-layer metasurfaces severely challenge their design and optimization. A universal strategy for the design of few-layer metasurfaces with different desired optical functionalities and an arbitrary number of layers, which can lower the design complexity and the time cost for structural optimization, is still eagerly anticipated by the scientific community. Here, we demonstrate an inverse design strategy based on deep-learning technology for the design of few-layer metasurfaces. By combining the matrix theory of multilayer optics, the proposed algorithm can predict the entire scattering matrix of a few-layer metasurface in tens of seconds with an acceptable accuracy and realize the inverse design of few-layer metasurfaces with different desired functionalities. Thus, the proposed inverse design strategy provides an efficient solution for the reduction of the design complexity of few-layer metasurfaces and significantly lowers the time cost for the structural optimization when compared with the numerical simulation methods based on an iterative process of trial and error, which will be of benefit to and expand the related research.

DOI: 10.1103/PhysRevApplied.17.024008

I. INTRODUCTION

Metasurfaces are planar periodic or nonperiodic arrays composed of subwavelength artificial nanostructures, which have been showing exceptional capabilities for single-dimensional and multidimensional manipulations of optical waves and provide a good alternative for the miniaturization and integration of optical devices [1–4]. One of the biggest challenges for metasurfaces is how to improve their working efficiency since the light-matter interaction between the metasurfaces composed of planar thin metallic nanostructures and optical waves is quite limited [5–7]. One way to tackle this challenge is utilizing the dielectric metasurfaces with both electric and magnetic resonances; the other way is using the few-layer designs [8–11].

Few-layer metasurfaces cannot be treated as the simple stacks of multiple monolayer metasurfaces; the ample mechanisms of the interlayer light-matter interactions result in the significant enhancement of the light-matter interactions between the thin metallic nanostructures and optical waves. Therefore, few-layer metasurfaces composed of more than one functional layer act as an appealing platform for the realization of high-efficient optical functionalities in broad or multiple bandwidths [12–16]. Moreover, the rich design freedoms of few-layer metasurfaces significantly expand the capabilities of few-layer metasurfaces for optical wave manipulation and the realization of alternative optical functionalities. Compared with monolayer ones, few-layer metasurfaces with unprecedented capabilities and flexibilities for optical wave manipulation have proved crucial for the realization of many optical functionalities. Recent advances indicate that few-layer metasurfaces offer great advantages for the

*Corresponding author. hcheng@nankai.edu.cn
†Corresponding author. schen@nankai.edu.cn

implementation of polarization conversion [17,18], asymmetric transmission [19,20], giant chiral optical response [21,22], high-efficient wavefront control [23–25], bidirectional perfect absorption [26,27], multifunctional integration [28,29], asymmetric and full-space optical wave manipulation [30–32], and so on. Despite the remarkable success that has been achieved, the rich design freedoms of few-layer metasurfaces severely challenge their design and optimization process, which is a major impediment to the development and application of few-layer metasurfaces. Nowadays, the primary objective for the optimization of metasurfaces is solving Maxwell's equations by utilizing numerical simulation based on the finite element method, the finite difference time domain method, and so on, which is an iterative process of trial and error. Compared with monolayer metasurfaces, few-layer metasurfaces have more degrees of design freedom, such as the number of layers, the layer-to-layer spacing, the structural symmetry, the constituent material, and the structural configuration of each layer. Therefore, the design and optimization of few-layer metasurfaces by utilizing numerical simulation are much more complex and time-consuming.

Benefiting from the rapid development of the big data technology and the machine learning method, a number of approaches have been proposed for the inverse design of metasurfaces, which can simplify the design process of metasurfaces and lower the time cost for structural optimization [33–36]. In these approaches, the desired optical response, as the input, is set as the optimization target by utilizing a cost function that describes the difference between the optical response of the optimized metasurface and the desired one, while the structural configuration of the metasurface whose optical response is equal or similar to the optimization target is the output. Recently, the inverse design of metasurfaces based on the neural network has attracted tremendous interest. Since metasurfaces with different structural configurations can have similar optical responses, design strategies based on the evolutionary algorithms, bidirectional neural networks, variational autoencoders, conditional variational autoencoders, and generative adversarial networks are widely utilized to solve the nonuniqueness problem and realize the inverse design of monolayer metasurfaces [37–44]. Recent advances further demonstrate the feasibility of the inverse design of the few-layer metasurfaces [45–49]. Despite the great progress that has been made with these approaches, they are not suitable for the realization of the inverse design of few-layer metasurfaces with different desired optical functionalities and an arbitrary number of layers, since some of them treat the nanostructures in different layers as a whole and the algorithm needs to be retrained for different optimization targets, while the others utilizing the adjoint and topology optimization method take much more time and also have fixed optimization targets.

Since neural network has a remarkable capacity for mapping the linear or nonlinear relationship between the input and the output, the inverse design method based on the neural network seems to be a good choice for the implementation of the inverse design of few-layer metasurfaces with different desired optical functionalities and an arbitrary number of layers. However, due to the rich design freedoms of few-layer metasurfaces, the build of the data set of few-layer metasurfaces for the training of the neural network and also the design and training of the neural network itself are very challenging, let alone the existence of the one-to-many mapping problem. Moreover, the necessary adjustment and retraining of the neural network for different optimization targets can also be time-consuming. A universal inverse design strategy with acceptable accuracy for the realization of the rapid inverse design of few-layer metasurfaces with any required optical functionalities still remains a challenge, which will be a great help for tackling the challenges in the design and optimization of few-layer metasurfaces.

Here, we provide an efficient inverse design strategy based on deep-learning technology for the realization of the rapid inverse design of few-layer metasurfaces with different required optical responses. By combing the matrix theory of multilayer optics and a convolutional neural network (CNN) simulator, the well-trained algorithm can predict the entire scattering matrix of a few-layer metasurface with acceptable accuracy. More importantly, the training of the CNN simulator only uses a data set of monolayer metasurfaces, which significantly reduces the difficulty of the data collection and makes the proposed algorithm become more scalable in the frequency domain. By further involving the evolution algorithm, the proposed algorithm can solve the one-to-many problem and realize the inverse design of few-layer metasurfaces with different optical responses. The proposed algorithm does not need to adjust and retrain the convolutional neural network for different optimization targets and different numbers of layers. The CNN simulator needs to be trained only once; then the proposed algorithm can realize the inverse design of few-layer metasurfaces with different required optical responses and an arbitrary number of layers. With a further experimental validation, we prove that the designed few-layer metasurfaces is manufacturable. The design strategy provides a powerful platform for the rapid design of few-layer metasurfaces with desired optical responses, which significantly reduces the design complexity of few-layer metasurfaces and lowers the time cost for the structural optimization when compared with the numerical simulation methods based on an iterative process of trial and error.

II. INVERSE DESIGN STRATEGY

The matrix theory of multilayer optics is utilized to tackle the challenge of the inverse design of few-layer

metasurfaces based on the neural network. It provides an efficient way to describe the scattering characteristics of a few-layer metasurface, under the condition that the near-field interactions between the layers are negligible. The matrix theory of multilayer optics has been widely used for the quantitative analysis of few-layer metasurfaces. And there is good consistency between the numerically calculated and experimentally measured results [12,15,20]. If the scattering matrices of every layer in a few-layer metasurface and the distance between adjacent layers are known, the whole scattering matrix of the few-layer metasurface can be directly calculated (details are given in Sec. (i) of the Supplemental Material [50]). By combing the matrix theory of multilayer optics and the CNN, we tackle the challenges for data set collection and the design and training of the convolutional neural network. Furthermore, by involving the evolutionary strategy in our inverse design strategy, we solve the nonuniqueness problem. The proposed strategy for the inverse design of few-layer metasurfaces contains three main components: a CNN simulator for the prediction of the scattering matrices of monolayer periodic metasurfaces, the wave-transfer matrix method for the calculation of the whole scattering matrix of the few-layer metasurface based on the predicted scattering matrices of the monolayer ones, and the evolution algorithm for finding the few-layer metasurface whose optical response is equal or close to the desired one.

As a proof of concept, an instance algorithm of the proposed strategy is shown in Fig. 1. The goal of the proposed algorithm is to realize the inverse design of few-layer metasurfaces composed of multiple layers of periodic aluminum nanostructures embed in a SU-8 substrate. The operating frequency band is set to 100–300 THz. The input of the algorithm is the distributions of several coefficients of the scattering matrix corresponding to the desired optical response; as an example, the input in Fig. 1 represents a broadband linear polarizer. The output of the

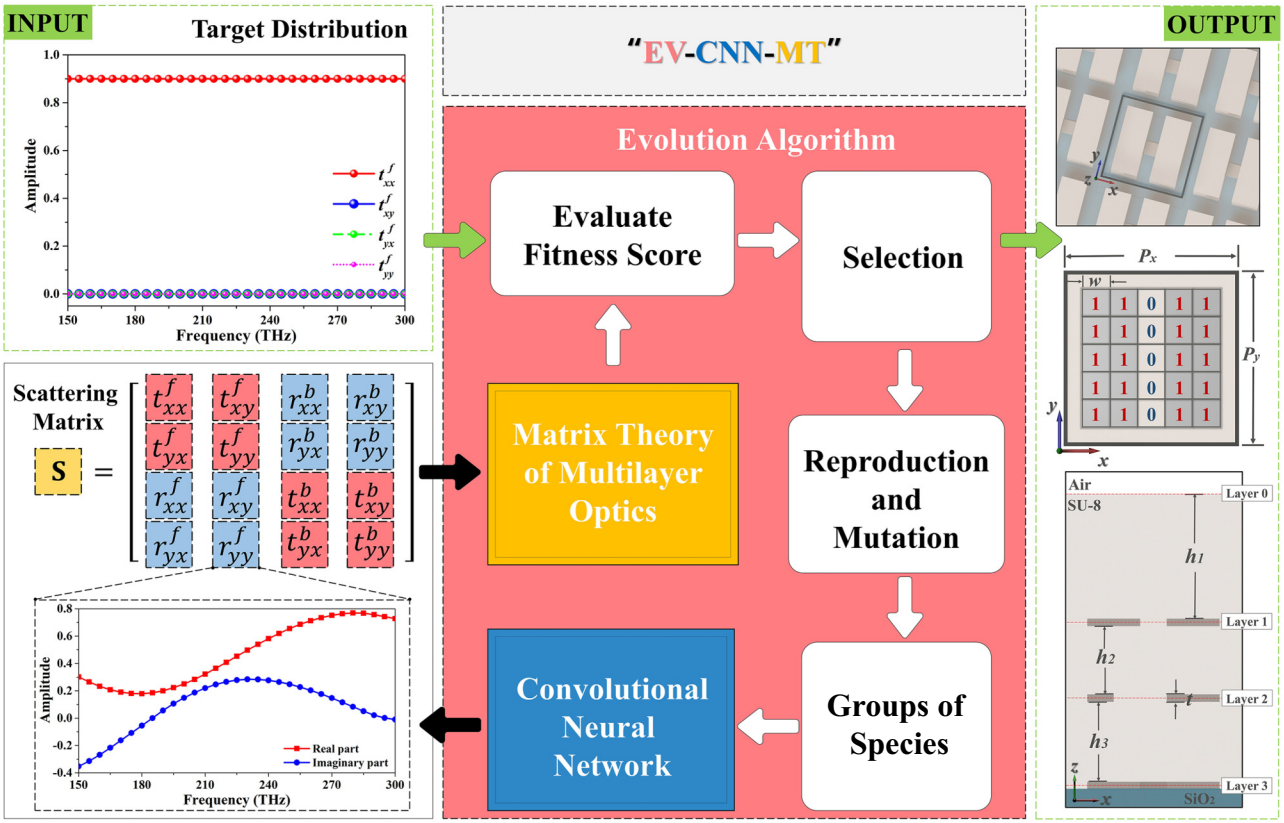

FIG. 1. Schematic diagram of the proposed "EV-CNN-MT" deep-learning algorithm built on the evolution algorithm, the convolutional neural network, and the matrix theory of multilayer optics, for the inverse design of few-layer metasurfaces with desired optical functionalities. The input is the target distributions of several coefficients of the scattering matrix, which represent the desired optical functionality. The output is the design detail of the few-layer metasurface whose optical response is equal or close to the desired one, including the structural configurations of each layer and the distance between the adjacent layers. The algorithm consists of three main components: the convolutional neural network simulator for the prediction of the scattering matrix of the monolayer periodic metasurface, the numerical model based on the matrix theory of multilayer optics for the calculation of the scattering matrix of the few-layer metasurface based on the predicted scattering matrices of the monolayer periodic ones, and the evolution algorithm for finding the few-layer metasurface whose optical response is equal or close to the desired one.

algorithm is the structural configuration of the designed few-layer metasurface whose optical response is equal or close to the desired one. It includes the structural configurations of the periodic unit cells in each layer and the distances between the adjacent layers. As shown in Fig. 1, the periodic nanostructures in every layer of the designed few-layer metasurface are composed of several aluminum cuboids, whose width $w = 70$ nm and thickness $t = 30$ nm. The periods of the unit cell in both the x and y directions are 450 nm. Each nanostructure can be represented by a 5×5 one-zero matrix. The structural configurations of the few-layer metasurfaces are designed with the consideration of the manufacturability based on the nanofabrication technologies, while the proposed inverse design strategy is universal for different constitute materials and structural configurations [16]. To realize the inverse design of few-layer metasurfaces, a CNN simulator needs to be designed and trained firstly for the prediction of the scattering matrices of monolayer metasurfaces with acceptable accuracy. In order to train the CNN simulator, we built up a data set of monolayer periodic metasurface, in which the features are the 5×5 one-zero matrices representing the structural configurations of monolayer metasurfaces composed of aluminum cuboids embed in the SU-8 substrate. The labels are their corresponding scattering matrices represented by 16×151 matrices. More details of the data collection process can be found in Sec. (ii) of the Supplemental Material [50]. We designed a CNN simulator and trained it with the built data set. By carefully adjusting the hyperparameters of the training process and the architecture of the CNN simulator, we obtain a well-trained CNN simulator that can predict the scattering matrix of a monolayer periodic metasurface with high accuracy. The details of the architecture of the CNN simulator and the training process can be found in Sec. (iii) of the Supplemental Material [50]. The performance of the CNN simulator is shown in Fig. 2. The inverse design of few-layer metasurfaces can be implemented after the training of the CNN simulator. The executed processes can be described as follows. First, a series of few-layer metasurfaces with different structural configurations are randomly generated. The scattering matrices of every monolayer in the generated few-layer metasurfaces are predicted by the well-trained CNN simulator. Then, the scattering matrices of the generated few-layer metasurfaces are obtained by utilizing the wave-transfer matrix method. The calculated scattering

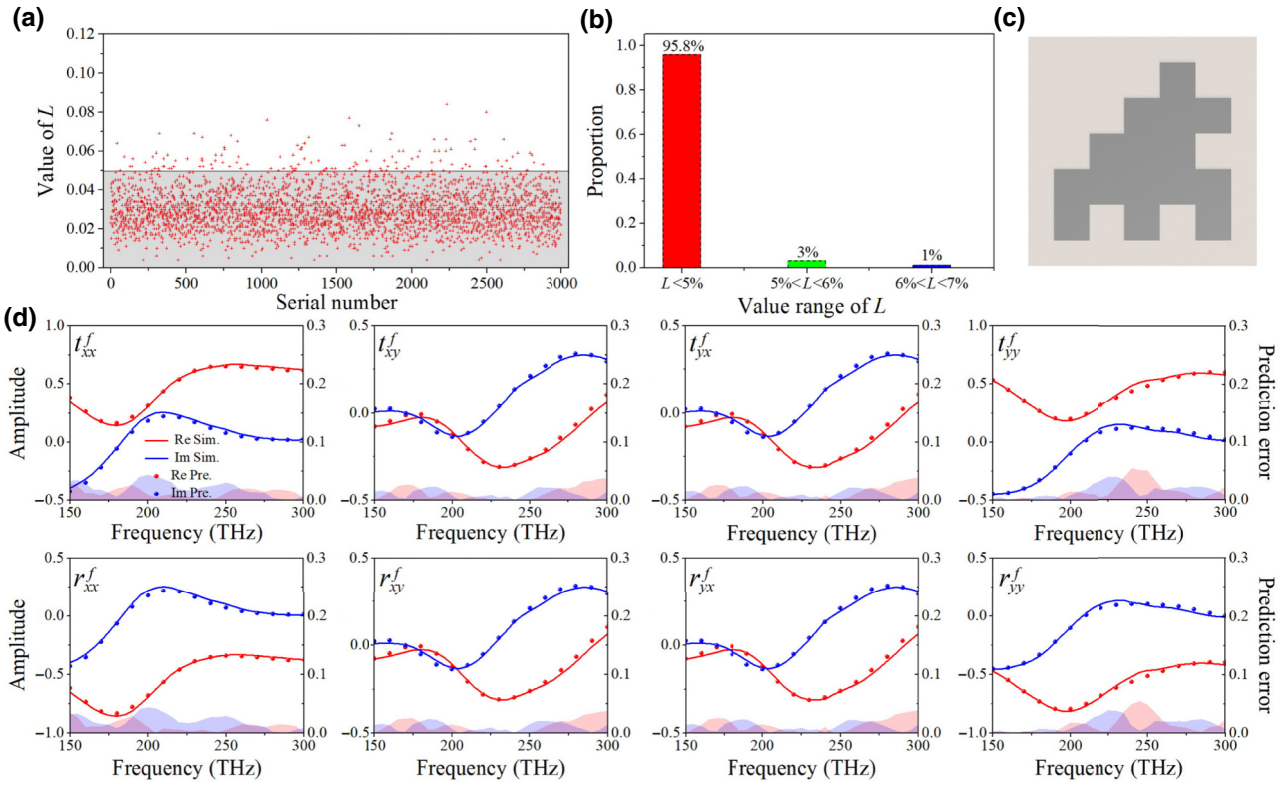

FIG. 2. Quantitative analysis on the performance of the well-trained CNN simulator. (a) The value L of the loss function for the individuals in the test data. (b) The proportion of the test data for which the value L of the loss function is in a different range. (c) A typical example of the unit cell of a monolayer periodic metasurface. (d) The predicted (dot plot) and simulated (line plot) results of the real and imaginary parts of the eight coefficients of the scattering matrix of the monolayer periodic metasurface in (c), and the corresponding calculated results of the prediction errors (area plot).

matrices of the generated few-layer metasurfaces are compared with the input by using the fitness function

$$S = \frac{1}{2MN}\sum_{i=1}^{M}\sum_{j=1}^{N}\{|\mathrm{Re}[S_i^{\mathrm{Pre}}(\lambda_j)] - \mathrm{Re}[S_i^{\mathrm{Obj}}(\lambda_j)]| + |\mathrm{Im}[S_i^{\mathrm{Pre}}(\lambda_j)] - \mathrm{Im}[S_i^{\mathrm{Obj}}(\lambda_j)]|\}, \quad (1)$$

where M and N represent the total number of the considered elements in the scattering matrix and the total number of the frequency points, respectively; $\mathrm{Re}(x)$ and $\mathrm{Im}(x)$ represent the real and imaginary parts of the complex number x; $S_i^{\mathrm{Pre}}(\lambda_j)$ and $S_i^{\mathrm{Obj}}(\lambda_j)$ represent the predictive and objective values of the ith element of the scattering matrix at the frequency point λ_j. Based on an appropriate evolutionary strategy, a new group of few-layer metasurfaces, whose optical responses are closer to the desired one, is generated after the selection, reproduction, and mutation processes. Then, we can obtain a few-layer metasurface after 60 cycles, whose optical response is close or equal to the desired one (the fitness function has a minimum value). If the number of layers of few-layer metasurfaces is less than five, the time cost for the inverse design of the few-layer metasurfaces will be less than one minute. The design and optimization process based on iterative numerical simulations is complex and time-consuming. The expended time depends on personal experience, which always take several hours, days, or weeks. Therefore, the proposed inverse design method is much faster than the design and optimization method based on an iterative process of trial and error. More details about the inverse design process and time cost can be found in Sec. (iv) of the Supplemental Material [50]. In order to validate the performance of the proposed algorithm, we next quantitatively analyze the performance of the well-trained CNN simulator and design several few-layer metasurfaces.

III. RESULTS AND DISCUSSION

The prediction accuracy of the CNN simulator plays a key role in the realization of the inverse design of few-layer metasurfaces. To quantitatively analyze the performance of the well-trained CNN simulator, 3000 samples from the data set are chosen as the test data. The prediction error of the CNN simulator representing the difference between the real and predicted scattering matrices of the monolayer metasurface can be expressed with the loss function

$$L = \frac{1}{2MN}\sum_{i=1}^{M}\sum_{j=1}^{N}\{|\mathrm{Re}[S_i^{\mathrm{Pre}}(\lambda_j)] - \mathrm{Re}[S_i^{\mathrm{Real}}(\lambda_j)]| + |\mathrm{Im}[S_i^{\mathrm{Pre}}(\lambda_j)] - \mathrm{Im}[S_i^{\mathrm{Real}}(\lambda_j)]|\}, \quad (2)$$

where M and N represent half of the total number of elements in the scattering matrix and the total number of the frequency points, equal to 8 and 151, respectively; $S_i^{\mathrm{Pre}}(\lambda_j)$ and $S_i^{\mathrm{Real}}(\lambda_j)$ represent the predicted and real values (numerical simulated results) of the ith element of the scattering matrix at the frequency point λ_j. The values of the loss function L for the test data are shown in Fig. 2(a). The corresponding statistical results are presented in Fig. 2(b). The results demonstrate that the scattering matrices of 95.8% test data can be well predicted while the corresponding values of the loss function (average errors) are less than 0.05. To make a more visual presentation of the performance of the well-trained CNN simulator, we provide the predicted and simulated results of the eight coefficients of the scattering matrix of a randomly generated monolayer periodic metasurface [as shown in Fig. 2(c)], and the corresponding calculated results of the prediction errors in Fig. 2(d). The prediction error is the absolute value of the difference between the predicted and simulated results. The difference between the predicted and the simulated scattering matrices for the monolayer metasurface is tiny. The maximum of the prediction error is around 0.05 for each coefficient. The results in Fig. 2 strongly prove that the well-trained CNN simulator can be used to realize the prediction of the scattering matrix of the monolayer metasurface with acceptable accuracy.

The efficiency of the inverse design strategy is firstly demonstrated by designing several bilayer metasurfaces with different optical functionalities, as shown in Fig. 3. Figure 3(a) shows the desired amplitude distribution of the transmission coefficient t_{xx}^f ($|t_{xx}^f|$ equals 0 from 150 to 220 THz, and $|t_{xx}^f|$ equals 1 from 240 to 300 THz), which represents the optical response of a polarization-dependent bandpass optical filter. The structural configuration of the inverse-designed bilayer metasurface is shown in Fig. 3(b). The predicted and simulated amplitude distributions of the transmission coefficient t_{xx}^f for the designed bilayer metasurface and the corresponding prediction error are shown in Figs. 3(c) and 3(d), respectively. Results indicate that the optical response of the inverse-designed bilayer metasurface is close to the desired one, and there is good agreement between the predicted and simulated results. Since the initialization and evolution processes are random, the structural configurations of the inverse-designed few-layer metasurfaces might be different in multiple runs. However, the optical responses of the inverse-designed few-layer metasurfaces are similar, which are close to the desired optical functionality (see Fig. S5 within the Supplemental Material [50]). Thus, the designers can choose from among many near-optimal structural configurations, based on criteria such as ease of fabrication. As another example, Fig. 3(e) shows the desired amplitude distributions of the

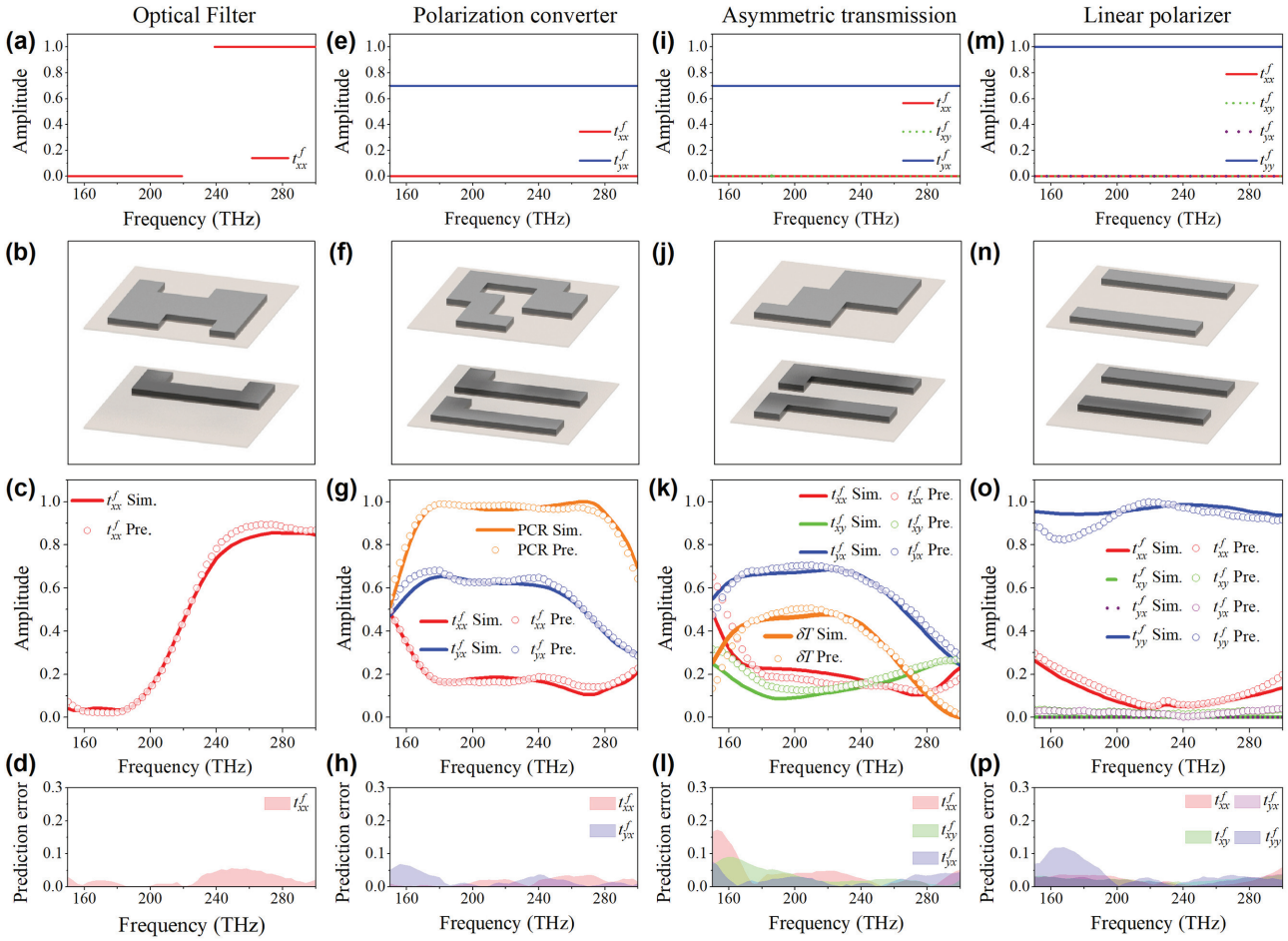

FIG. 3. Inverse design of bilayer metasurfaces with different optical functionalities based on the proposed deep-learning algorithm. Inverse design of a bilayer metasurface as a bandpass optical filter for x-polarized waves: (a) the target amplitude distribution of t_{xx}^f corresponding to the desired functionality; (b) the structural configuration of the inverse-designed bilayer metasurface; (c) the simulated and the predicted results; and (d) the prediction error (difference between the predicted and the simulated results) of the amplitude distribution of t_{xx}^f for the designed bilayer metasurface. Inverse design of a bilayer metasurface as a broadband polarization convertor for x-polarized waves: (e) the target amplitude distribution of t_{xx}^f and t_{yx}^f corresponding to the desired functionality; (f) the structural configuration of the inverse-designed bilayer metasurface; (g) the simulated and the predicted results; and (h) the prediction error of the amplitude distribution of t_{xx}^f and t_{yx}^f for the designed bilayer metasurface, and the corresponding calculated results of the PCR. Inverse design of a bilayer metasurface to realize the diodelike asymmetric transmission of the x-polarized waves: (i) the target amplitude distribution of t_{xx}^f, t_{xy}^f, and t_{yx}^f corresponding to the desired functionality; (j) the structural configuration of the inverse-designed bilayer metasurface; (k) the simulated and the predicted results; and (l) the prediction error of the amplitude distribution of t_{xx}^f, t_{xy}^f, and t_{yx}^f for the designed bilayer metasurface, and the corresponding calculated results of the transmission difference δT. Inverse design of a bilayer metasurface as a broadband linear-polarizer: (m) the target amplitude distribution of t_{xx}^f, t_{xy}^f, t_{yx}^f, and t_{yy}^f corresponding to the desired functionality; (n) the structural configuration of the inverse-designed bilayer metasurface; (o) the simulated and the predicted results; and (p) the prediction error of the amplitude distribution of t_{xx}^f, t_{xy}^f, t_{yx}^f, and t_{yy}^f for the designed bilayer metasurface.

transmission coefficient t_{xx}^f and t_{yx}^f ($|t_{xx}^f|$ equals 0 from 150 to 300 THz, while $|t_{yx}^f|$ equals 0.7 in the whole operation waveband), which represent the optical response of a broadband cross-polarization converter. Here $|t_{yx}^f|$ is set to be equal to 0.7 since the polarization conversion efficiency in previous bilayer metasurfaces is lower than 40% [51]. The structural configuration of the inverse-designed bilayer metasurface is given in Fig. 3(f). The predicted and simulated amplitude distributions of the transmission coefficients t_{xx}^f and t_{yx}^f for the designed bilayer metasurface, and the corresponding prediction error are shown in Figs. 3(g) and 3(h), respectively. The designed bilayer metasurface can be treated as a linear cross-polarization converter from 170 to 280 THz with polarization conversion rate (PCR)

over 90%, as shown in Fig. 3(g). The PCR is defined as

$$\eta_{\mathrm{PCR}} = \frac{|t^f_{yx}|^2}{|t^f_{xx}|^2 + |t^f_{yx}|^2}. \tag{3}$$

Figures 3(g) and 3(h) further prove that the predicted results are in good agreement with the simulated ones. Moreover, there is a certain difference between the optical response of the inverse-designed bilayer metasurface and the desired one. It might be attributed to the inexistence of the bilayer metasurface whose optical response meets the desired one. This difference can also be observed from the results in Figs. 3(i)–3(l). The desired amplitude distributions of the transmission coefficients t^f_{xx}, t^f_{xy}, and t^f_{yx} represent the diodelike asymmetric transmission of linear-polarized waves in the whole operation waveband, which is unique in few-layer metasurfaces and cannot be realized in monolayer metasurfaces [16]. Figure 3(k) indicates that the optical response of the designed bilayer metasurface can partially satisfy the desired target with acceptable prediction accuracy. The designed bilayer metasurface can realize the asymmetric transmission of x-polarized optical waves from 170 to 240 THz with transmission difference δT over 40%. Here, the δT is defined as $\delta T = |t^f_{yx}|^2 - |t^f_{xy}|^2$ [20]. However, the diodelike asymmetric transmission cannot be realized since $|t^f_{xy}|$ and $|t^f_{xx}|$ are not equal to zero in the whole bandwidth. This result reflects that the algorithm can find the bilayer metasurfaces for which the fitness function has a minimum value, but the designed bilayer metasurfaces might not have enough diversity and capacity to fulfill the desired target. Fortunately, this drawback can be overcome by involving another degree of design freedom (that is, the number of layers) in few-layer metasurfaces. Moreover, the proposed algorithm can obtain the whole scattering matrix of the designed few-layer metasurface at every run (see Fig. S6 within the Supplemental Material [50]). Thus, other optical functionalities that can be represented by the distribution of the coefficients of the scattering matrix can also be realized by using the proposed inverse design strategy. To further make a comparison between the proposed inverse design strategy and the numerical optimization method in our previous work, we designed a broadband linear polarizer with the proposed algorithm, as shown in Figs. 3(m)–3(p). Figures 3(n) and 3(o) demonstrate that the inverse-designed bilayer metasurface can be treated as a linear polarizer from 190 to 280 THz since the transmittance of the x-polarized waves is lower than 1%. Compared with our previous bilayer design [15], the proposed bilayer metasurface has a broader operation waveband and a comparable efficiency. Figures 3(m)–3(p) further demonstrate the validity of the inverse design strategy through comparisons with the numerical optimization method. The simulated and predicted results have a visible difference at some frequency points for some transmission coefficients, which can be seen in Figs. 3(k) and 3(o). This is mainly attributed to the prediction error of the CNN simulator (see Figs. S7 and S8 within the Supplemental Material [50]). An improvement of the prediction accuracy of the CNN simulator will further increase the accuracy of the inverse design algorithm. The details of the structural configurations of the designed bilayer metasurfaces in Fig. 3 can be found in Fig. S9 of the Supplemental Material [50].

Not only the bilayer metasurfaces, but also the few-layer metasurfaces with an arbitrary number of layers can be inversely designed by the proposed algorithm. We designed several few-layer metasurfaces with different numbers of layers to realize the diodelike asymmetric transmission of x-polarized waves in the whole operation bandwidth, as shown in Fig. 4. To realize the desired optical functionality, the target amplitude distributions of t^f_{xx}, t^f_{xy}, and t^f_{yx} are set as $|t^f_{xx}|$ and $|t^f_{xy}|$ equal to 0 from 150 to 300 THz while $|t^f_{yx}|$ equals 0.9. Figure 4(a) gives the structural configurations of the designed few-layer metasurfaces with different numbers of layers (details of their structural configurations can be found in Fig. S10 of the Supplemental Material [50]). The simulated and predicted amplitude distributions of t^f_{xx}, t^f_{xy}, and t^f_{yx} for the designed few-layer metasurfaces and the corresponding calculated prediction errors are shown in Figs. 4(b)–4(e) and 4(f)–4(i), respectively. Results show that the proposed algorithm can realize the prediction of the optical responses of few-layer metasurfaces with different numbers of layers. The mean error is less than 5%. As shown in Fig. 4(b), the diodelike asymmetric transmission of x-polarized waves cannot be realized by the designed bilayer metasurface since $|t^f_{xy}|$ and $|t^f_{xx}|$ are not equal to zero in the whole bandwidth, as we mentioned above. When the number of layers increases, $|t^f_{xy}|$ and $|t^f_{xx}|$ get closer and closer to zero, as shown in Figs. 4(b)–4(e). The designed few-layer metasurfaces with four and five layers can well realize the diodelike asymmetric transmission of x-polarized waves in a broad bandwidth. The optical responses of the designed few-layer metasurfaces get closer to the desired one as the number of layers increases, which plays a critical role in the design of few-layer metasurfaces. Despite that few-layer metasurfaces composed of several layers with planar nanostructures can be fabricated based on the well-established top-down electron-beam lithography technique [11,16], the number of layers should not be excessive as the existence of ohmic losses and the cost and accuracy limitation of fabrication technology. Specially, although every layer of the few-layer metasurfaces is independently fabricated and the optical responses of few-layer metasurfaces designed based on the matrix theory of multilayer optics is robustness to the misalignment between the layers, the accumulated fabrication errors from all the layers will significantly

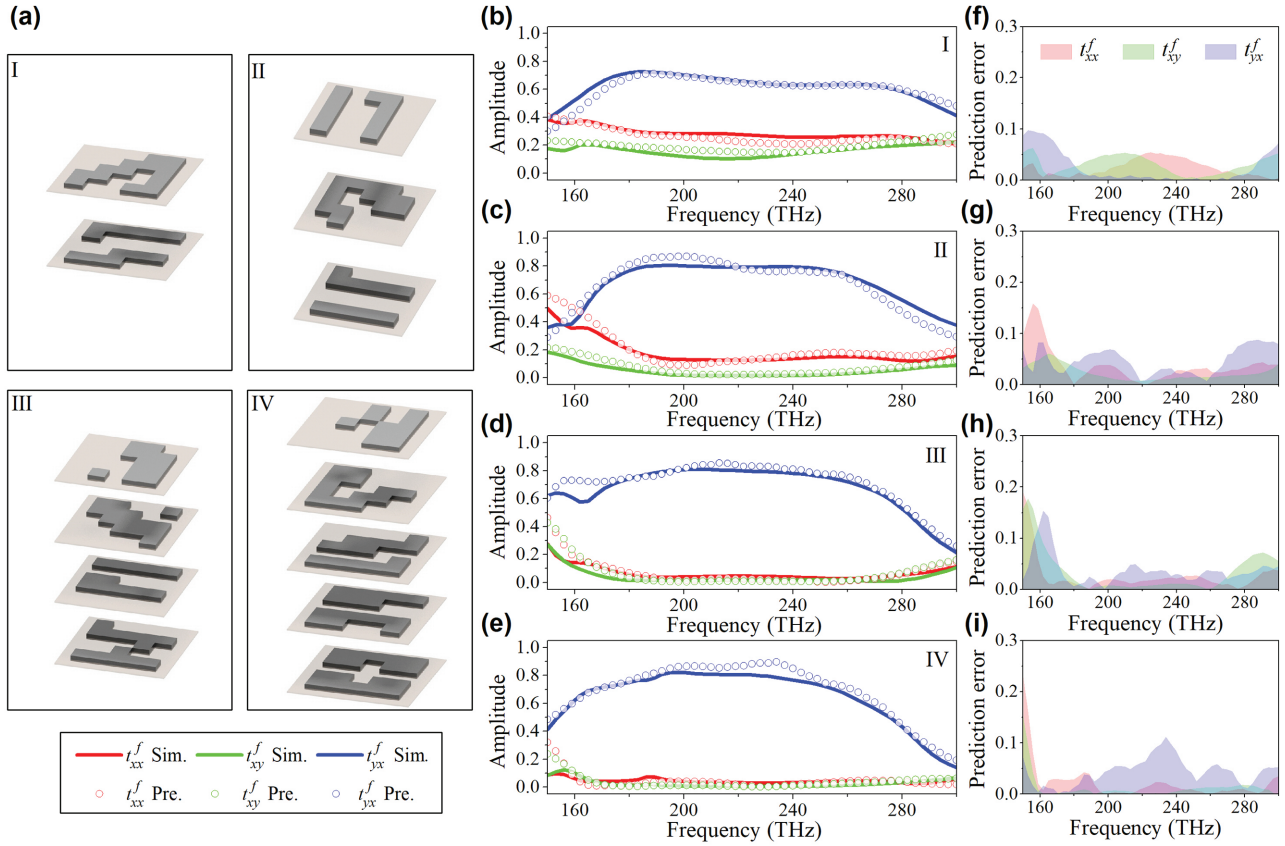

FIG. 4. Inverse design of the few-layer metasurfaces with the same optical functionalities and different numbers of layers based on the proposed deep-learning algorithm. The few-layer metasurfaces are inversely designed to realize the diodelike asymmetric transmission of x-polarized optical waves with the operation frequency from 150 to 300 THz, that is, the amplitude distribution of t_{xx}^f, t_{xy}^f, and t_{yx}^f are $|t_{xx}^f| = 0$, $|t_{xy}^f| = 0$, and $|t_{yx}^f| = 0.9$ from 150 to 300 THz. (a) The structural configuration of the inverse-designed few-layer metasurface with different numbers of layers. (b)–(e) The simulated and the predicted results and (f)–(i) the prediction error of the amplitude distribution of t_{xx}^f, t_{xy}^f, and t_{yx}^f for the designed few-layer metasurface.

affect the optical properties of the few-layer metasurface as the number of layers increases. In this sense, the proposed inverse design strategy, which can find a few-layer metasurface with desired optical responses and a minimum number of layers, provides a powerful means for the selection of the number of layers in the design of few-layer metasurfaces.

Since the manufacturability of the structural configurations is considered during the design, the inverse-designed few-layer metasurfaces can be fabricated by the well-established technique in nanofabrication. As a proof of concept, two bilayer metasurfaces, which can be treated as broadband linear polarizers, are fabricated to make an experimental validation. The structural configurations of the fabricated bilayer metasurfaces are shown in Figs. 5(a) and 5(e), and the corresponding scanning electron microscope (SEM) images are shown in Figs. 5(b) and 5(f), respectively (details of their structural configurations can be found in Fig. S11 of the Supplemental Material [50]). The bilayer metasurface in Fig. 5(a) is the same as the inverse-designed bilayer metasurface in Fig. 3(n), which can be treated as a near-perfect linear polarizer from 190 to 280 THz. The bilayer metasurface in Fig. 5(e) can be treated as a near-perfect linear polarizer from 210 to 230 THz, where the target amplitude distributions of t_{xx}^f, t_{xy}^f, t_{yx}^f, and t_{yy}^f for the inverse design are set as $|t_{xx}^f|$, $|t_{xy}^f|$, and $|t_{yx}^f|$ equal to 0 from 200 to 240 THz while $|t_{yy}^f|$ equals 0.9. The simulated and predicted transmission intensities $T_{ij} = |t_{ij}|^2$ in Figs. 5(c) and 5(g) are in reasonable agreement with the experimental results in Figs. 5(d) and 5(h), respectively. This indicates that the optical responses of the fabricated samples of the inverse-designed metasurfaces are close to the desired ones. The differences between the simulated and experimental results are attributed to the structural differences due to fabricational tolerances. As limited by the precision of our existing nanofabrication process, the fabrication imperfection of the edge of the aluminum cuboids is significant, as shown in Figs. 5(b) and 5(f). For inverse-designed metasurfaces whose optical

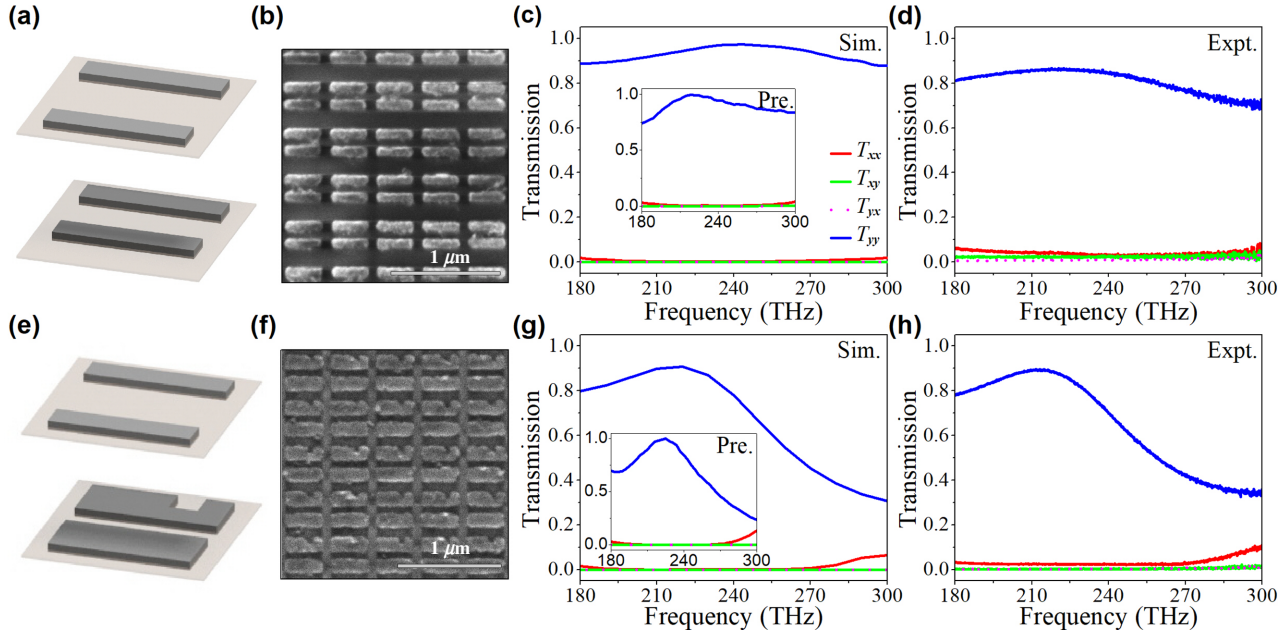

FIG. 5. Experimental validation of the optical responses of the two inverse-designed few-layer metasurfaces that can be treated as broadband linear polarizers. (a) The structural configuration of one inverse-designed few-layer metasurface and its (b) SEM image of the upper layer, and the (c) simulated results, predicted results, and (d) experimental results of the transmission spectra ($T_{ij} = |t_{ij}|^2$) for the designed few-layer metasurface. (e) The structural configuration of the other inverse-designed few-layer metasurface and its (f) SEM image of the lower layer, and the (g) simulated results, predicted results, and (d) experimental results of the transmission spectra for the designed few-layer metasurface.

responses are sensitive to this fabrication imperfection (for example, metasurfaces with strong field enhanced at the edge of the aluminum cuboids) or with complex structural configurations (especially for those whose structural configurations include isolate aluminum cuboids, such as that in Fig. 4(a), III), the fabricated samples show poor performance. Thus, improving the precision of the nanofabrication technology and optimizing the structural configuration of the monolayer metasurface will be of benefit to the real application of the proposed algorithm in the near-infrared band.

With the combination of matrix theory of multilayer optics, the convolutional neural network, and the evolution algorithm, the proposed EV-CNN-MT deep-learning algorithm provides a universal strategy for the inverse design of few-layer metasurfaces. Compared with previous inverse design approaches in which the targets are always one or two fixed optical characteristics (such as the transmission or reflection spectrum, circular dichroism, and so on) [36–49], the proposed strategy is universally applicable, which can be used to realize the inverse design of few-layer metasurfaces with different desired optical functionalities and an arbitrary number of layers. The proposed algorithm overcomes the great challenges faced by the neural-network-based inverse design of few-layer metasurfaces in the building of the data set and the design and training of the neural network, which show the following advantages. (1) Since few-layer metasurfaces have much more design freedom when compared with monolayer ones, it is quite difficult to build a required data set for the training of the neural network. Our proposed inverse design strategy does not need a data set of few-layer metasurfaces for the training of the algorithm. Instead, a data set of monolayer metasurfaces is built as the data set for the training of a CNN simulator. With the well-trained CNN simulator, the optical response of a few-layer metasurface with an arbitrary number of layers can be obtained based on the matrix theory of multilayer optics. (2) Few-layer metasurfaces with different structural configurations can show similar optical response. This one-to-many mapping problem is solved by utilizing the evolution algorithm in our proposed inverse design strategy. On the one hand, the evolution algorithm can find the few-layer metasurface whose optical response can meet or is close to the on-demand optical functionality in every run. Even if there is no such few-layer metasurface whose optical response can fully satisfy the required optical functionality, the few-layer metasurface whose optical response is close to the on-demand functionality can also be obtained. On the other hand, since the initialization and evolution process are random, the inversely designed few-layer metasurfaces by multiple runs will be different for a required optical functionality (see Fig. S5 within the Supplemental Material [50]). However, the optical responses of the

few-layer metasurfaces obtained by multiple runs are similar, which are close to the required optical functionality. Thus, the designers can choose from among many near-optimal structural configurations, based on criteria such as ease of fabrication. (3) For previous inverse design approaches in which the targets are always focused on one or two fixed optical characteristics, the neural networks need to be adjusted and retrained when the optimization target is changed, which is time-consuming. On the contrary, the proposed algorithm can predict the entire scattering matrix of a few-layer metasurface with an arbitrary number of layers in a broad bandwidth within an acceptable prediction error range (see Fig. S6 within the Supplemental Material [50]). It means that the proposed algorithm does not need to adjust and retrain the convolutional neural network for different optimization targets and different numbers of layers, which can be used to realize versatile optical functionalities [16]. The proposed design strategy can further be used to implement the inverse design of an aperiodic few-layer metasurface by designing the unit cell one by one [52]. (4) The proposed algorithm is a powerful platform for the design of few-layer metasurfaces since almost all degrees of the design freedom (structural symmetry, number of layers, layer-to-layer spacing, structural configuration of each layer) are involved in the inverse design process. Since the data set for the training of the algorithm is only based on aluminum nanostructures, the current proposed algorithm does not address the case where different layers are constituted with different materials. The inverse design of few-layer metasurfaces with different materials in each layer can be further realized by involving several training data sets with different materials for nanostructures.

Certainly, the proposed inverse design strategy also has several limitations. (1) The matrix theory of multilayer optics is feasible for the calculation of the scattering matrices of few-layer metasurfaces when the near-field interaction between the layers is negligible. Thus, the layer-to-layer spacing in the proposed algorithm is set to be larger than 120 nm (distance-dependent near-field splitting is very weak) to make sure that the impact of the near-field interaction is negligible. It means that the near-field interaction effect, which is an important degree of the design freedom in few-layer metasurfaces, is not involved in this inverse design process. (2) With the consideration of manufacturability, the designed planar nanostructure in each layer, which can be represented by a 5×5 zero-one matrix, is composed of several isolate aluminum cuboids with 70 nm width. Thus, the diversity of the planar nanostructure in each layer is limited. A more reasonable method for the generation of the planar nanostructure is highly desirable for the build of the training data set [37]. (3) Since the scattering matrices of the few-layer metasurfaces are calculated by the predicted scattering matrices of each layer, the prediction errors of the scattering matrices of the monolayers will significantly affect the prediction accuracy of the scattering matrices of the few-layer metasurfaces (see Figs. S7 and S8 within the Supplemental Material [50]). Therefore, although the CNN simulator is well trained, the prediction accuracy of the CNN simulator needs to be further improved for the inverse design of few-layer metasurfaces with many layers.

IV. CONCLUSION

In conclusion, we implement the inverse design of few-layer metasurfaces based on the combination of the deep-learning technology and a physical model of light-matter interaction. The inverse design algorithm consists of three main parts: the CNN simulator for the prediction of the scattering matrix of the monolayer periodic metasurface, the numerical model based on the matrix theory of multilayer optics for the calculation of the scattering matrix of the few-layer metasurface, and the evolution algorithm for finding the few-layer metasurface whose optical response is equal or close to the desired one. With both numerical and experimental validation, the efficiency of the proposed algorithm has been well proved. The greatest advantage of the proposed algorithm is that we do not need to adjust and retrain the convolutional neural network for different optimization targets and different numbers of layers. Thus, the inverse design strategy provides a powerful platform for the rapid design of few-layer metasurfaces with different optical responses, which significantly reduces the design complexity of few-layer metasurfaces and lowers the time cost for the structural optimization when compared with the numerical simulation methods based on an iterative process of trial and error. We believe that the proposed design strategy will lower the knowledge requirement for the design of few-layer metasurfaces, which will be of benefit to researchers and engineers, and make the design of few-layer metasurfaces more convenient and faster.

ACKNOWLEDGMENTS

Z.L. thanks Zhaocheng Liu and Wenshan Cai for useful programming support, suggestions, and comments. This work is supported by the National Key Research and Development Program of China (Grants No. 2021YFA1400601 and No. 2017YFA0303800), the National Natural Science Fund for Distinguished Young Scholar (Grant No. 11925403), the National Natural Science Foundation of China (Grants No. 12122406, No. 12192253, No. 11974193, No. 11904181, and No. 11904183), the Natural Science Foundation of Tianjin for Distinguished Young Scientists (Grant No. 18JCJQJC45700), and the China Postdoctoral Science Foundation (Grant No. 2018M640224). The work was partly performed at the ACT node of the Australian National Fabrication Facility.

[1] H. H. Hsiao and D. P. Tsai, Fundamentals and applications of metasurfaces, Small Methods **1**, 1600064 (2017).

[2] X. Luo, D. P. Tsai, M. Gu, and M. Hong, Subwavelength interference of light on structured surfaces, Adv. Opt. Photonics **10**, 757 (2018).

[3] X. Luo, Subwavelength artificial structures: Opening a new era for engineering optics, Adv. Mater. **31**, 1804680 (2019).

[4] S. Chen, Z. Li, W. Liu, H. Cheng, and J. Tian, From single-dimensional to multidimensional manipulation of optical waves with metasurfaces, Adv. Mater. **31**, 1802458 (2019).

[5] X. Ni, N. K. Emani, A. V. Kildishev, A. Boltasseva, and V. M. Shalaev, Broadband light bending with plasmonic nanoantennas, Science **335**, 427 (2012).

[6] W. Wan, J. Gao, and X. Yang, Full-color plasmonic metasurface holograms, ACS Nano **10**, 10671 (2016).

[7] W. Liu, S. Chen, Z. Li, H. Cheng, P. Yu, J. Li, and J. Tian, Realization of broadband cross-polarization conversion in transmission mode in the terahertz region using a single-layer metasurface, Opt. Lett. **40**, 3185 (2015).

[8] S. Jahani and Z. Jacob, All-dielectric metamaterials, Nat. Nanotechnol. **11**, 23 (2016).

[9] I. Staude and J. Schilling, Metamaterial-inspired silicon nanophotonics, Nat. Photonics **11**, 274 (2017).

[10] H. Cheng, Z. Liu, S. Chen, and J. Tian, Emergent functionality and controllability in few-layer metasurfaces, Adv. Mater. **27**, 5410 (2015).

[11] S. Chen, Y. Zhang, Z. Li, H. Cheng, and J. Tian, Empowered layer effects and prominent properties in few-layer metasurfaces, Adv. Opt. Mater. **7**, 1801477 (2019).

[12] N. K. Grady, J. E. Heyes, D. R. Chowdhury, Y. Zeng, M. T. Reiten, A. K. Azad, A. J. Taylor, D. A. R. Dalvit, and H. T. Chen, Terahertz metamaterials for linear polarization conversion and anomalous refraction, Science **340**, 1304 (2013).

[13] C. Pfeiffer, C. Zhang, V. Ray, L. J. Guo, and A. Grbic, Polarization rotation with ultra-thin bianisotropic metasurfaces, Optica **3**, 427 (2016).

[14] W. Luo, S. Sun, H. X. Xu, Q. He, and L. Zhou, Transmissive Ultrathin Pancharatnam-Berry Metasurfaces with Nearly 100% Efficiency., Phys. Rev. Appl. **7**, 044033 (2017).

[15] Z. Li, W. Liu, H. Cheng, D. Y. Choi, S. Chen, and J. Tian, Arbitrary manipulation of light intensity by bilayer aluminum metasurfaces, Adv. Opt. Mater. **7**, 1900260 (2019).

[16] Z. Li, W. Liu, H. Cheng, and S. Chen, Few-layer metasurfaces with arbitrary scattering properties, Sci. Chin. Phys. Mech. **63**, 284202 (2020).

[17] Y. Nakata, Y. Taira, T. Nakanishi, and F. Miyamaru, Free-standing transparent terahertz half-wave plate using sub-wavelength cut-wire pairs, Opt. Express **25**, 2107 (2017).

[18] C. P. Huang, Y. Zhang, Y. L. Wang, and L. B. Kong, Arbitrarily Directional and Tunable Polarization Rotating Effect with Coupled Metal Screens, Phys. Rev. Appl. **10**, 064038 (2018).

[19] J. H. Shi, H. F. Ma, C. Y. Guan, Z. P. Wang, and T. J. Cui, Broadband chirality and asymmetric transmission in ultra-thin 90-twisted babinet-inverted metasurfaces, Phys. Rev. B **89**, 165128 (2014).

[20] J. Liu, Z. Li, W. Liu, H. Cheng, S. Chen, and J. Tian, High-efficiency mutual dual-band asymmetric transmission of circularly polarized waves with few-layer anisotropic metasurfaces, Adv. Opt. Mater. **4**, 2028 (2016).

[21] Y. Cui, L. Kang, S. Lan, S. Rodrigues, and W. Cai, Giant chiral optical response from a twisted-arc metamaterial, Nano Lett. **14**, 1021 (2014).

[22] Z. Li, W. Liu, H. Cheng, S. Chen, and J. Tian, Spin-selective transmission and devisable chirality in two-layer metasurfaces, Sci. Rep. **7**, 8204 (2017).

[23] H. X. Xu, L. Han, Y. Li, Y. Sun, J. Zhao, S. Zhang, and C. W. Qiu, Completely spin-decoupled dual-phase hybrid metasurfaces for arbitrary wavefront control, ACS Photonics **6**, 211 (2018).

[24] J. Zhang, M. ElKabbash, R. Wei, S. C. Singh, B. Lam, and C. Guo, Plasmonic metasurfaces with 42.3% transmission efficiency in the visible, Light: Sci. Appl. **8**, 53 (2019).

[25] M. Jia, Z. Wang, H. Li, X. Wang, W. Luo, S. Sun, Y. Zhang, Q. He, and L. Zhou, Efficient manipulations of circularly polarized terahertz waves with transmissive metasurfaces, Light: Sci. Appl. **8**, 16 (2019).

[26] J. Li, P. Yu, C. Tang, H. Cheng, J. Li, S. Chen, and J. Tian, Bidirectional perfect absorber using free substrate plasmonic metasurfaces, Adv. Opt. Mater. **5**, 1700152 (2017).

[27] Z. Li, W. Liu, C. Tang, H. Cheng, Z. Li, Y. Zhang, J. Li, S. Chen, and J. Tian, A bilayer plasmonic metasurface for polarization-insensitive bidirectional perfect absorption, Adv. Theor. Simul. **3**, 1900216 (2020).

[28] T. Cai, S. Tang, G. Wang, H. Xu, S. Sun, Q. He, and L. Zhou, High-performance bifunctional metasurfaces in transmission and reflection geometries, Adv. Opt. Mater. **5**, 1600506 (2017).

[29] T. Cai, G. M. Wang, H. X. Xu, S. W. Tang, H. Li, J. G. Liang, and Y. Q. Zhuang, Bifunctional pancharatnam-berry metasurface with high-efficiency helicity-dependent transmissions and reflections, Ann. Phys.-Berlin **530**, 1700321 (2018).

[30] D. Frese, Q. Wei, Y. Wang, L. Huang, and T. Zentgraf, Nonreciprocal asymmetric polarization encryption by layered plasmonic metasurfaces, Nano Lett. **19**, 3976 (2019).

[31] T. Cai, G. Wang, S. Tang, H. Xu, J. Duan, H. Guo, F. Guan, S. Sun, Q. He, and L. Zhou, High-Efficiency and Full-Space Manipulation of Electromagnetic Wave Fronts with Metasurfaces, Phys. Rev. Appl. **8**, 034033 (2017).

[32] Z. Li, W. Liu, H. Cheng, J. Liu, S. Chen, and J. Tian, Simultaneous generation of high-efficiency broadband asymmetric anomalous refraction and reflection waves with few-layer anisotropic metasurface, Sci. Rep. **6**, 35485 (2016).

[33] W. Ma, Z. Liu, Z. A. Kudyshev, A. Boltasseva, W. Cai, and Y. Liu, Deep learning for the design of photonic structures, Nat. Photonics **15**, 77 (2020).

[34] S. Molesky, Z. Lin, A. Y. Piggott, W. Jin, J. Vucković, and A. W. Rodriguez, Inverse design in nanophotonics, Nat. Photonics **12**, 659 (2018).

[35] M. M. Elsawy, S. Lanteri, R. Duvigneau, J. A. Fan, and P. Genevet, Numerical optimization methods for metasurfaces, Laser Photonics Rev. **14**, 1900445 (2020).

[36] R. Pestourie, C. Pérez-Arancibia, Z. Lin, W. Shin, F. Capasso, and S. G. Johnson, Inverse design of large-area metasurfaces, Opt. Express **26**, 33732 (2018).

[37] Z. Liu, D. Zhu, S. P. Rodrigues, K. T. Lee, and W. Cai, Generative model for the inverse design of metasurfaces, Nano Lett. **18**, 6570 (2018).

[38] N. Bonod, S. Bidault, G. W. Burr, and M. Mivelle, Evolutionary optimization of all-dielectric magnetic nanoantennas, Adv. Opt. Mater. **7**, 1900121 (2019).

[39] C. C. Nadell, B. Huang, J. M. Malof, and W. J. Padilla, Deep learning for accelerated all-dielectric metasurface design, Opt. Express **27**, 27523 (2019).

[40] L. Gao, X. Li, D. Liu, L. Wang, and Z. Yu, A bidirectional deep neural network for accurate silicon color design, Adv. Mater. **31**, 1905467 (2019).

[41] T. Qiu, X. Shi, J. Wang, Y. Li, S. Qu, Q. Cheng, T. Cui, and S. Sui, Deep learning: A rapid and efficient route to automatic metasurface design, Adv. Sci. **6**, 1900128 (2019).

[42] Y. Li, Y. Xu, M. Jiang, B. Li, T. Han, C. Chi, F. Lin, B. Shen, X. Zhu, L. Lai, and Z. Fang, Self-Learning Perfect Optical Chirality via a Deep Neural Network, Phys. Rev. Lett. **123**, 213902 (2019).

[43] I. Malkiel, M. Mrejen, A. Nagler, U. Arieli, L. Wolf, and H. Suchowski, Plasmonic nanostructure design and characterization via deep learning, Light: Sci. Appl. **7**, 60 (2018).

[44] T. Phan, D. Sell, E. W. Wang, S. Doshay, K. Edee, J. Yang, and J. A. Fan, High-efficiency, large-area, topology-optimized metasurfaces, Light: Sci. Appl. **8**, 48 (2019).

[45] W. Ma, F. Cheng, and Y. Liu, Deep-learning-enabled on-demand design of chiral metamaterials, ACS Nano **12**, 6326 (2018).

[46] W. Ma, F. Cheng, Y. Xu, Q. Wen, and Y. Liu, Probabilistic representation and inverse design of metamaterials based on a deep generative model with semi-supervised learning strategy, Adv. Mater. **31**, 1901111 (2019).

[47] A. S. Backer, Computational inverse design for cascaded systems of metasurface optics, Opt. Express **27**, 30308 (2019).

[48] M. Mansouree, H. Kwon, E. Arbabi, A. McClung, A. Faraon, and A. Arbabi, Multifunctional 2.5 D metastructures enabled by adjoint optimization, Optica **7**, 77 (2020).

[49] H. Chung and O. D. Miller, Tunable metasurface inverse design for 80% switching efficiencies and 144 angular deflection, ACS Photonics **7**, 2236 (2020).

[50] See Supplemental Material at http://link.aps.org/supplemental/10.1103/PhysRevApplied.17.024008 for (i) the matrix theory of multilayer optics, (ii) data collection for the training of the CNN simulator, (iii) architecture of the CNN simulator and the training details, (iv) details of the evolution strategy, (v) data supporting the discussion of the advantages and limitations of the proposed algorithm, (vi) structural configurations of the designed metasurfaces in Figs. 3–5, and (vii) sample fabrication and measurement methods. The advanced Jones calculus supporting the discussion in (i) and (ii) can be found in Reference [12] and the literature: C. Menzel, C. Rockstuhl, and F. Lederer, Advanced Jones calculus for the classification of periodic metamaterials, Phys. Rev. A **82**, 053811 (2010). The optical constants of aluminum used in (ii) for data collection were taken from: E. D. Palik, *Handbook of Optical Constants of Solids* (Academic Press, New York, 1998).

[51] Z. Li, S. Chen, W. Liu, H. Cheng, Z. Liu, J. Li, P. Yu, B. Xie, and J. Tian, High performance broadband asymmetric polarization conversion due to polarization-dependent reflection, Plasmonics **10**, 1703 (2015).

[52] D. Zhu, Z. Liu, L. Raju, A. S. Kim, and W. Cai, Building multifunctional metasystems via algorithmic construction, ACS Nano **15**, 2318 (2021).